Lorrey Andrew (Orcid ID: 0000-0002-3923-3181)

Full Title: Southwest Pacific atmospheric weather regimes: linkages to ENSO and extra-tropical teleconnections

Short Title: Southwest Pacific weather regimes: linkages to ENSO and teleconnections

Andrew M. Lorrey [1]
Nicolas C. Fauchereau [2]

1 National Institute of Water and Atmospheric Research, Auckland, New Zealand
2 National Institute of Water and Atmospheric Research, Hamilton, New Zealand

This work was sponsored by the Royal Society of New Zealand Marsden Fund project "Detecting prehistoric human-climate dynamics in central Polynesia using high-precision marine archives". Co-funding for AML and NCF time for analysis also came from the NIWA core-funded project "Climate Present and Past" project CAOA1701 and National Oceanic and Atmospheric Administration support for "The South Pacific Rainfall Atlas (SPRAT)".

Southwest Pacific atmospheric weather regimes: linkages to ENSO and extra-tropical teleconnections

Abstract

We objectively identified an optimal number of atmospheric weather regimes, also called synoptic types, within the southwest Pacific tropical-subtropical domain and examined their potential drivers. Six atmospheric weather regimes in this region are characterized by spatially heterogeneous geopotential height, sea surface temperature and regional precipitation patterns, they are phase-locked to the seasonal cycle with a moderate degree of coherency, and some are capable of persisting for weeks or more in extreme cases. Correlations between the southwest Pacific weather regimes and global precipitation reanalysis fields indicate a strong connection between regional weather patterns and South Pacific Convergence Zone (SPCZ) mean position changes and relative intensity of convective loci within the SPCZ. Climate field correlations to weather regimes show distinct geopotential height and SST signatures across Southern Hemisphere middle and high latitudes and the Indian Ocean basin. Strong statistical significance for portions of those spatial patterns lend support to the assertion of extra-basin teleconnections for southwest Pacific weather regimes. There are strong precipitation impacts from SW Pacific weather regime frequency changes and regime persistence on extreme rainfall deficits and/or surpluses for small islands during austral summer. Diagnostic analysis of the spatial correlation fields and each weather regime

indicates unique weather patterns are connected to eastern equatorial Pacific-styles of El Niño and La Niña, and Modoki La Niña. Another regime type appears to be connected to an enhancement of the Hadley-Ferrell circulation, while two other types are influenced by phenomena that arise outside the Pacific Basin (Madden-Julian Oscillation, Southern Annular Mode, and Pacific South American mode). SW Pacific weather regime investigations in the context of modern climate, palaeoclimatology, and future climate change scenarios can help to surmount spatial scale mismatches that exist between global models and small islands, while helping to improve general understanding of island-scale impacts from atmospheric circulation.

1. Introduction

Previous work has shown regional-scale daily weather patterns that characterise the near-surface atmospheric circulation (i.e. synoptic circulation) can be decomposed into discrete and recurrent archetypes called “atmospheric circulation regimes” or “weather regimes” (WR thereafter). WRs are an important paradigm for extra-tropical weather and climate research because they can be interpreted as dynamical attractor basins in phase space that is visited by atmospheric circulation (Mo and Ghil, 1988; Vautard and Legras, 1988; Kimoto, 1989; Vautard, 1990).

Synoptic weather typing has been successful in the Northern Hemisphere (NH), where multiple studies have applied a range of clustering algorithms to daily atmospheric

circulation data sets as a way to derive regionally-prominent WRs (Mo and Ghil, 1988; Vautard, 1990; Michelangeli et al. 1995; Cassou, 2008). In many cases, WRs correspond to large-scale climate modes (i.e. North Atlantic Oscillation; NAO+, NAO- phases) and other regionally-specific geographic patterns (i.e. 'Atlantic Ridge' WR and a 'Scandinavian Blocking' WR), which can influence their frequency of occurrence.

Regional climate anomalies (e.g. temperature and rainfall) in Europe are demonstrated to arise from changes in the occupation statistics of WRs that are modulated by large-scale climate modes that operate at intra-seasonal to inter-annual time-scales (see e.g. Yiou and Nogaj, 2004). As such, the prediction potential of hydroclimatic impacts beyond weather time-scales (Baldwin and Dunkerton, 2001) can be enabled by a better understanding of weather regime behavior.

Elsewhere, linkages between daily meteorological conditions from WRs and seasonal-to-intra-seasonal variability show connections to climate phenomenon such as the monsoon (Qian et al., 2012), Madden-Julian Oscillation (MJO; Cassou, 2008; Fauchereau et al., 2016) and El Niño-Southern Oscillation activity (ENSO; Moron and Plaut, 2003; Moron et al., 2015). However, with respect to NH continental regions, WR research has been less applied in the tropics than in the extra-tropics. Because tropical circulation is dominated by convective activity and boundary forcings (e.g. sea surface temperature anomalies) that are inherently more important than in the extra-tropics, the

dynamical interpretation of WRs is less clear than in extra-tropical circulation situations.

There is limited application of WR work for the SW Pacific or the tropics elsewhere (Kidson, 2000; Lefevre et al., 2010; Ackerley et al., 2011; Renwick, 2011; Jiang et al., 2014; Moron et al., 2016), but the studies that do exist demonstrate they can critically improve understanding of climate driver impacts, including those from ENSO. The spatial displacement and changes in convection for the Intertropical Convergence Zone (ITCZ) and South Pacific Convergence Zone (SPCZ; Matthews, 2012; Widlansky et al., 2011) during ENSO events, for example, have notable effects on Pacific Island rainfall. They also can influence regional patterns of tropical cyclone occurrence (Diamond et al., 2013) and extra-tropical transition of tropical cyclones (Lorrey et al., 2014b) that can impact the lives of millions of people. As such, there is a significant impetus to better understand WRs in the SW Pacific.

In this paper, we undertake a synoptic weather typing exercise that is applied to the southwest Pacific Basin (10˚N - 30˚S, 160˚E - 130˚W; see section 3.1 for test of domain results). The inevitable choice of domain was motivated by the importance of the SW Pacific in the global climate system and by the large degree of regional climate variability – and associated detrimental impacts – that affect the Pacific Islands (e.g. drought, deluge and tropical cyclones; Lorrey and Renwick, 2011; Diamond et al., 2013). We expect that a WR view of atmospheric circulation variability in the SW

Pacific will contextualize interpretations of past weather and climate events and improve prediction of regional and local impacts of atmospheric circulation regimes from weather to seasonal timescales.

2. Methods

2.1 Data

2.1.1 Climate fields

We determined South Pacific (SP) WRs using daily geopotential heights from NCEP/NCAR1 (see Kalnay et al, 1996) over the period spanning the 1 January 1950 to 31 December 2014 (February 29 removed on leap years). Monthly averages of the zonal (U) and meridional (V) components of 850 and 200 hPa were also obtained for analysis (see http://www.esrl.noaa.gov/psd/data/gridded/data.ncep.reanalysis.html). Monthly sea surface temperatures were derived from the ERSSTv3b Dataset, available over the 1948-2014 period at a monthly time resolution and over a 2x2 degree grid (downloaded from ftp://ftp.ncdc.noaa.gov/pub/data/cmb/ersst/v4/netcdf).

Monthly rainfall anomalies were also calculated from the Global Precipitation Climatology Project (GPCP) dataset (version 2, Adler et al, 2003) which merges data from rain gauge stations, satellites, and sounding observations on a 2.5-degree global grid from 1979 to the present. For all spatial data drawn from these reanalysis data sets,

the long-term (linear) trend was removed prior to further analysis. All monthly anomalies were calculated with respect to the 1981-2010 climatology to be consistent with the treatment of the other datasets and indices.

2.1.2 Climate indices

The Coupled ENSO index (CEI) was initially developed by Gergis and Fowler (2005) as a way to indicate the relative strength and alignment of key atmospheric and oceanic indicators of ENSO. We have adopted that style of classification and recalculated the CEI over the period 1950 – 2014 from the original SOI and NIÑO3.4 values, with anomalies calculated with respect to the 1981 – 2010 climatology.

The SOI is first calculated from the raw mean sea level pressure (MSLP) data for Tahiti (T) and Darwin (D) made available online by the Australian Bureau of Meteorology (BoM) at ftp://ftp.bom.gov.au/anon/home/ncc/www/sco/soi. The SOI is calculated following the Troup (Troup, 1965) method as:

$$SOI = [\,(T - Tc) - (D - Dc)\,] \,/\, [\,StDev\,(T - D)\,] \quad (1)$$

The 1981-2010 climatological averages for Tahiti (Tc) and Darwin (Dc) surface pressures and StDev is the standard deviation of the MSLP difference between these two locations.

The CEI uses the NIÑO3.4 temperature anomalies in the central-western equatorial Pacific [5˚S– 5˚N, 120˚W–170˚W] for its oceanic component. The monthly NIÑO3.4 sea surface temperatures index from the ERSSTv3b Dataset were used, and are made available by the Climate Prediction Center at http://www.cpc.ncep.noaa.gov/data/indices/ersst3b.Niño.mth.81-10.ascii.

Running averages (3 months for the SOI, 5 months for the NIÑO3.4 index) are then calculated, the CEI being defined as:

$$CEI = (SOI * -1) + NIÑO3.4 \quad (2)$$

The CEI categories are defined according to simultaneous values of the SOI and the NIÑO3.4, whereby if both the SOI and NIÑO3.4 exceed set thresholds for El Niño (La Niña), it is termed a CEI NIÑO (NIÑA) event. Likewise, an ocean-dominated event is indicated when only the NIÑO3.4 index exceed the threshold, and similarly for atmospheric-dominated event. The oceanic thresholds used for NIÑO3.4 are +/- 0.5 °C for the five-month mean and the SOI threshold is +/- 1.0 standard deviations for the three-month mean. A previous classification of ENSO events using the CEI and comparison to other ENSO classification schemes are found in Gergis and Fowler (2005).

It has been recognized over the past decades that there are more than three simple states of ENSO (positive, neutral, negative). Leading paradigms indicate there is a continuum of ENSO composed of different typologies (Capotondi et al., 2015), with ENSO phases occurring in more than one "flavor" that have main distinctions related to the longitude of the maximum SST anomalies along the Equator (Johnson, 2013). For the latter perspective, 'canonical' ENSO flavors can have SST spatial anomalies that are strongly centered in the far eastern and far western equatorial Pacific, while a more recently recognized ENSO variation shows core anomalies for the 'eastern pole' that are centered closer to the International Dateline. This latter type of ENSO has been referred to in the literature as the ''dateline El Niño'' (Larkin and Harrison 2005), ''El Niño Modoki'' (Ashok et al. 2007), ''warm pool El Niño'' (Kug et al. 2009), and ''central Pacific El Niño'' (Yeh et al. 2009). We use a measure of ENSO called the El Niño 'Modoki' (EMI) index that has been calculated from the ERSST SST anomalies (1981 – 2010 climatological normal) by Ashok et al (2007) as:

$$EMI = [SSTA]A - 0.5*[SSTA]B - 0.5*[SSTA]C \quad (3)$$

The square bracket represents the "area-averaged SST anomalies (SSTa)" over segments of the central Equatorial Pacific, divided into sub regions A (165˚E-140˚W, 10˚S-10˚N), B (110˚W-70˚W, 15˚S-5˚N), and C (125˚E-145˚E, 10˚S-20˚N), respectively. We further divide the EMI in three categories: '*EMI* +', '*EMI* –' and '*Neutral*', using +/- one standard deviations as thresholds.

We focus on the two aforementioned indices and use them to assess the sensitivity of WR frequency with regard to the co-occurring ocean – atmosphere conditions for ENSO events (as seen through the CEI) as well as the 'flavor' of ENSO ('canonical' or eastern Pacific type of ENSO vs. 'Modoki' or central Pacific type of ENSO) via the EMI.

2.1.3. Station rainfall data

Historic monthly rainfall returns from the Pacific Islands Meteorological Services that are held in NIWA's climate database are utilized. High-quality stations with less than 2% missing monthly data for 1950-2014 were selected from that database, and rainfall totals (in mm) and percent rainfall anomalies relative to the 1981-2010 climatology interval were calculated. The December-February monthly mean anomalies were then averaged together to produce a mean seasonal anomaly values. All seasonal mean calculations were required to have at least two of the three-month totals present (or else they were omitted).

2.2. Analyses

2.2.1 Cluster analysis: test of domain area and spatial field

Daily anomalies of geopotential height at 1000hPa, 850hPa, 500hPa, and 200hPa (z1000, z850, z500, and z200) for several discrete areas of the South Pacific domain

were evaluated with respect to the 1981-2010 climatic normal period. These anomalies were subjected to Empirical Orthogonal Function (EOF) decomposition, and the first eight Principal Components (PCs), which explained up to 80% of the original variance, were retained to form the reduced space within which the clustering procedures were applied.

One of the caveats of most clustering algorithms is that *a-priori* assignment of the number of clusters (K) must be made. However, it is usually unclear what the 'optimal' number of clusters is for climate datasets. Recently, the so-called Affinity Propagation (AP) algorithm has been introduced (Frey and Dueck, 2007). The AP algorithm is based on the concept of "message passing" between data points, and uses the dissimilarity matrix as an input. Unlike clustering algorithms such as *k*-means or *k*-medoids (Kaufman and Rousseeuw, 1990; Park and Jun, 2009) AP does not require the number of clusters to be determined *a-priori*. Like *k*-medoids, AP finds "exemplars"; these are members of the input set that are representative of clusters, and the AP assigns each point in the given data set to the closest exemplar.

A drawback of this algorithm is its complexity and associated computing requirements. AP has a time complexity of the order $O^*(N^2*T)$, where N is the number of samples and T is the number of iterations until convergence. Furthermore, the memory complexity is of the order $O^*(N^2)$. In the present study N = 23725 days (daily data over the 1st January 1950 – 31 December 2014 period), which makes using AP directly for determination of

the WRs prohibitive. We therefore adopted a Monte-Carlo approach to determine the optimal partition (optimal number of WRs): we applied AP repeatedly (P = 1000) on samples (size N = 2000) drawn from the original dataset (i.e. the base formed by the aforementioned 8 PCs). Any natural partition of this dataset should emerge as a peak in the distribution of K amongst the P iterations. Once the latter is determined, the standard – and computationally efficient – *k*-means clustering algorithm (Hartigan, 1975, Michelangeli et al, 1995) can then be applied to yield the set of WRs.

2.2.2 Relationship to climate modes

In accord with previous work (Moron & Plaut, 2003; Cassou, 2008; Riddle et al., 2013; Moron et al., 2015) we investigated how the occupation statistics (*i.e.* the probability of occurrence) of South Pacific WRs are modulated by large-scale, slow varying climate modes. Our main focus was ENSO, with a particular interest on the relationships of each WR to different styles of co-occurring ocean – atmosphere conditions for ENSO events. Because of the phase-locking of ENSO to the annual cycle (Tziperman et al., 1994) and the presence of a seasonal component in the distribution of the WR (see Figure 3 in Section 2.1), there is a need to account for both the phase of ENSO and the time of the year with regard to WR frequency. We applied overlapping three-month windows (i.e. DJF, JFM etc.) calculations of each WR frequency and attributed the calculated statistics (*e.g.* probability of occurrence of the WRs or transition probabilities) to the middle month (e.g. January indicates the value for DJF) when plotted through time.

2.2.3 Significance of the occupation statistics changes for WRs

From a statistical standpoint, the time-sequence of WR occurrence can be summarized by the number of days each WR is observed over the period considered, which also is used to show probabilities of transitioning from one WR to the next. The WR transition probabilities includes persistence (probability of 'staying' in the same WR). This perspective closely corresponds to the definition of a Discrete Time Markov Chain (DTMC; Wilks, 2011).

The information that is encapsulated by WR probabilities and transition matrices lend to DTMC being employed as the basis of a Monte-Carlo significance test. This test requires generation of an arbitrary number of time-series of the discrete WRs of any length, whose statistical properties are virtually identical to the observed time series (when long periods are considered). Our application of this tactic is essentially similar to the methodology exposed in Riddle et al. (2013), Lorrey et al. (2014) and Fauchereau et al. (2016). Specifically, and using an example with the CEI, 10000 artificial time-series of WRs occurrences were performed independently for each season (DJF, JFM etc.) and CEI phase (7 categories, see Section 2.1). The change in probability (compared to the observed climatological occurrences) of observing a given WR is then calculated for each of the 10000 synthetic realizations. The 95 % confidence limit is drawn from this null distribution, so that the observed anomaly in the frequency of a WR is considered significant at the 95 % confidence level if it is below the corresponding simulated 5^{th} percentile for negative anomalies (above the 95^{th} percentile for positive anomalies).

3. Results

3.1 Cluster analysis test of domain area and spatial field

The WR domain was considered for a discrete spatial area that would adequately capture variations in both the position and intensity of the South Pacific Convergence Zone (SPCZ). Our reasoning for this choice is because the SPCZ has prominent

influences on Pacific Island rainfall on inter-seasonal timescales. There are strong connections between the SPCZ and ENSO (Vincent et al., 2011), which have direct impacts on regional sea surface temperatures and the atmospheric circulation properties. The SPCZ region of definition has previously been ascribed by Widlansky et al. (2010), and it extends from Papua New Guinea to French Polynesia. In essence, the choice of including larger or smaller areas around the core SPCZ zone are somewhat arbitrary, but whatever WRs can be defined should remain relatively insensitive to an subtle shifts in the domain size and location. As such, we tested four different spatial domains *(1: [-40, 0, 140, 230], 2: [-40, 0, 160, 230], 3: [-30, 10, 150, 220], 4: [-30, 10, 160, 230])* that included the core area of SPCZ activity and also the equatorial region of ENSO SST activity (Supplementary Figure 1) prior to undertaking a full suite of in depth analyses. We also evaluated whether discrete WR archetypes at different atmospheric levels achieved different optimal values.

The results of that antecedent evaluation indicated that z1000 leads to the most compact representation of daily atmospheric circulation across all of our selected spatial domains, with the optimal number of weather regime clusters increasing with altitude through the atmosphere. As such, z1000 was used for further assessment on the sensitivity of domain spatial choice. The distribution of Ks as determined by affinity propagation for the 1000 iterations (see Section 2.1) indicated the optimal number of WRs is between three and nine, with a local peak of six types (Figure 1). The computationally-efficient *k*-means clustering algorithm was then applied specifying

K=6, for the four different test spatial domains. When we cross-correlated the resultant spatial field patterns for each WR cluster according to the chosen spatial domain (1-3 = test domains, 4 = control domain), each of the six discrete weather regimes were found for every southwest Pacific domain choice, regardless of whether the analysis domain was shifted south and east by 10 degrees or even expanded either south or westward (even by up to 20 degrees of longitude). As such, we used the results of z1000 for domain 4 *[-30, 10, 160, 230]* to ascribe regional weather regimes for the SW Pacific, and the domain choice closely follows a region circumscribing the SPCZ (Widlansky et al., 2010). The composite daily z1000 geopotential anomalies (relative to 1981-2010 climatic normal base period) for each of the six WRs, as well as the number of days they are observed show the main spatial characteristics of regional atmospheric circulation and the resultant near-surface wind field patterns (Figure 2).

As in previous WR studies (Kidson, 2000), the spatial locations of geopotential height anomalies in the domain can be used to describe each regime and the circulation across the area of interest. We provide preliminary descriptors for each of these regimes here, but continue to refer to them in the text in their numeric format. A majority of the regimes contain low-pressure anomalies that are situated in different locations, on average, within the chosen domain. WR1 has a distinct high-pressure anomaly over the SW Pacific (hence named "HSP"-type), WR2 has a moderately-strong low pressure centre to the east of the International Date Line in the subtropics (subtropical low, or "STL"-type), and a high pressure anomaly to the southwest of it in the North Tasman

Sea, lending to enhanced westerly-to-northerly quarter flow across many islands. WR3 sees more frequent troughs in the North Tasman Sea ("TNT"-type) and an associated wind flow pattern across the domain that is largely opposite of WR6, which has a deep low (trough) over French Polynesia ("TFP"-type). WR4 shows spatial traits that are essentially an amplification of equatorial low pressure and mid latitude high pressure belts (enhanced climatological pattern or "EC"-type). WR5 shows a strong trough to the northeast of New Zealand ("TNZ"-type) and a high pressure anomaly south of the Austral Islands that produces stronger meridional flow across many SW Pacific islands.

3.2 WR climatological properties

While the seasonal cycle and long term trend have been removed from the daily z1000 time-series prior to the clustering procedure, the *distribution* of most WRs presents some degree of seasonality. For the climatology (1981-2010) of WR occurrence on a three-monthly basis (Figure 3, plotted by central month), WR5 and WR6 occur more frequently during the austral cool and dry season (May-October). WR2 tends to occur more frequently during the austral summer season (December-February) while.WR3 sees a gradual increase in frequency from austral summer through the following austral spring. WR2 has the strongest amplitude in terms of frequency change over the course of a year, while WR1 has the lowest amplitude for changes in frequency, occurring almost uniformly throughout the year.

3.3 Persistence and transitions

The distribution of WR sequence length (number of consecutive days a WR is observed), the transition probabilities (i.e. difference between the observed transition probabilities and what would be expected given the overall frequency of the WRs), and prevalence of self-transitions across the annual cycle were calculated for all seasons over the 1981-2010 period (Figure 4a, 4b, 4c). WR persistence metrics are summarized in Figure 4.

The distribution of the consecutive sequence length is positively skewed for all WRs. Most of the regimes last two or three days, and rare occurrences of SP WR sequences can last multiple weeks (Figure 4). WR4 is the most persistent regime on average (~3.3 days) and has a moderately long maximum sequence length (20 days). WR1 and WR6 have the longest maximum observed persistence (26 days) compared to the other WRs (Figure 4a). The longest consecutive sequence is observed for WR1 and WR6, with one WR1 sequence lasting 26 consecutive days from 25 January 2011 to 19 February 2011 and one for WR6 that lasted from 10 January to 4 February 1998.

Figure 4b presents the observed transitions from one WR to another, expressed as deviations of their expected probability relative to the overall frequency of each WR occurrence in the observed record. For example, the transition from WR3 to WR5 is 83.5% more frequent than what could be expected by chance only given the frequency of WR5 in the period of observation. Some preferred transition paths are evident (e.g.

the sequence WR2 to WR6 and WR3 to WR5 are more frequent than what could be expected by chance). On the other hand, some transitions and transition paths are "highly unlikely" (far less frequent than what one could expect by chance). Examples of this are the transition WR3 to WR4 and WR2 to WR4; both at least 40% less frequent that what could be expected by chance. While beyond the scope of this particular study, these preferred or unlikely transition paths have implications in terms of predictability at the sub-seasonal time-scale.

For most of the WRs that have been identified in this study, there is a higher prevalence of self-transition (i.e. persistence) during the months of the year (February and March) when tropical SSTs are at their highest (and conversely when persistence is lowest). The exception to this is seen for WR5, which has a relatively stable degree of self-transition through the year (Figure 4c).

3.4 Relationships to the large-scale climate background state

The relationships between inter-annual variability of SP WRs and large-scale climate conditions are assessed using the correlation fields for monthly WR frequency anomalies versus monthly sea-surface temperature anomalies (SSTa; Figure 5) and 850hPa geopotential anomalies (z850; Figure 6).

Overall, SSTa (Figure 5) and z850 (Figure 6) spatial correlations for three of the WR (1, 3, 6) are configured in an arrangement reminiscent of ocean and atmosphere patterns

typically associated with ENSO. WR1 and WR3 have correlation patterns that are akin to the spatial expression of two types of La Niña (Song et al., 2017). WR1 has SSTa correlations along the Equator that are strongest to the east of the International Date Line. WR3 has correlations to SST along the Equator that appear strongest west of the International Date Line along with much stronger subtropical and extra-tropical SST correlations than WR1. WR3 and WR6 have largely opposite geopotential correlation signatures from the tropics to the high southern latitudes, which (along with other metrics) suggest they represent opposite ENSO phases (see further explanation in Section 3.5). WR1 has spatial correlations for SSTs that appear similar to the ENSO-like SST correlations for WR3 but the correlation field pattern appears weaker across the Pacific, and the distribution of the positive and negative correlations outside of the Pacific Basin also appear different from WR3. In addition, the spatial correlation pattern seen in the z850 field for WR1 does not look like what is observed for WR3 (or its counterpart WR6; Figure 6), which has a more typical atmospheric mass 'see-saw' pattern for northern Australia/Maritime Continent and French Polynesia, potentially in conjunction with a pattern similar to what may be observed for the Pacific South American mode. Overall, the strongest SST correlations (Figure 5) for all six weather regimes are found in the central and sub-tropical Pacific basin, while weaker correlations (for most regimes, except WR1, 3, 6, and weakly for WR5) are observed in the higher latitudes and in the Indian Ocean basin.

While SST correlations appear weak and inconsistent for WR2, 4 and WR5 (Figure 5b, 5d, and 5e, respectively), their z850 spatial correlations (see Figure 6b, 6d, and 6e) have strong signatures. WR4 has a z850 correlation pattern that is similar to the climatological expression of an enhanced Hadley/Ferrell cell circulation. The strongest negative correlations for that regime are orientated in a zonal pattern along the equator (akin to the region of low pressure where the Hadley circulation rises) and are accompanied by positive correlations along the middle latitudes of both hemispheres in the locations where the Hadley and Ferrell cells descend to generate a high pressure belt).

WR2 and WR5 both have weak correlations to SSTa in general, but show some very isolated locations where SST correlations are significant. The former regime is associated with positive z850 correlations (higher-than-normal geopotential height) over New Zealand and lower-than-normal pressure northeast of New Zealand in the subtropics close to the International Date Line (approximately where Fiji, Samoa, Niue, and Tonga are located). The latter regime, when increased in frequency, is associated with north-central Tasman Sea low-pressure intensification (Figure 6) and cooler SST anomalies in the same area (Figure 5).

Correlations between WR monthly frequency anomalies and monthly SST anomalies at the Equator in the Pacific basin between 120°E and the South American coast (Figure 7;

calculated using ERSSTv3c at 2° longitudinal increments) shows that WR6 has peak SST correlations at about 160°W and mostly strong correlations to the east of that location (a pattern corresponding to eastern Pacific types of El Niño). Both WR1 and WR3 have strong SST correlations for the central and western Pacific, but WR3 SSTa correlations are consistently stronger than WR1 eastward from 170°E. Both WR2 and WR4 are poorly correlated to SSTs in the central Pacific.. WR4 only has strong correlations to equatorial SSTa 20 degrees either side of the International Date Line.

3.5 Relationships between WR and ENSO indices

Changes in WR probability for CEI phases (neutral phase is omitted for the sake of brevity: no significant modulations are found) along the seasonal cycle (Figure 8) show ocean-dominated ENSO events (NIÑO3.4 El Niño or NIÑO3.4 La Niña) are generally not associated with any significant WR frequency changes, bar a subtle increase in WR6 during austral summer-autumn. Conversely, both the atmosphere-dominated (SOI NIÑO / SOI NIÑA) and ocean-atmosphere aligned ENSO events (CEI NIÑO and CEI NIÑA) identified using the CEI indicate significant modulation of some WR frequencies. Overall, WR4 and WR5 do not appear to have appreciable correlations to the CEI, and only negative correlations for WR2 (i.e. a regime decrease) are only observed during SOI NIÑO events (Figure 8).

Prominent asymmetries for specific WR occurrences and for their preferred timing are highlighted for two main regime examples (WR3 and WR6; see section 3.4) that are

suggested to have ENSO connections (Figure 8). WR3 is strongly decreased during CEI NIÑO (mainly during the austral spring, summer and autumn period) but the same regime has weak increases during CEI NIÑA (for all times of the year except for DJF-FMA). Conversely, WR6 increases in association with CEI NIÑO and SOI NIÑO phases, and it has a nearly opposite (symmetric) response (decrease in frequency) during CEI NIÑA and SOI NIÑA (Figure 8).

Interestingly WR1 is also positively associated with SOI NIÑA and it has similar correlation patterns for SSTa as what is observed for WR3 (Figure 5c). However, WR1 and WR3 have very different Pacific-wide geopotential patterns (Figure 6a and 6c). This shows that WRs with highly distinct atmospheric circulation patterns can be favored during the same ENSO phase, and can also partly explain the variability of impacts between ENSO events of the same sign and similar magnitude as measured by only one index.

The changes in WR probability as a function of the EMI state ('neutral' category omitted because only weak and insignificant relationships were identified) and the phase of the seasonal cycle indicate the strongest and most significant frequency changes occur for WR1 (Figure 9). Increased occurrence of WR1, mostly during the SH late summer, autumn, winter, and early spring correspond to negative EMI phases (when SSTs in the central Pacific are anomalously cold). Conversely, during EMI

positive phases, there is a much weaker change in the frequency of WR1 than what is observed during EMI negative conditions (Figure 9). WR3 has a robust positive frequency change when negative EMI conditions exist. It appears to strengthen during the time of the year (November-January and December-February) when no other observed strong relationships exist for the other WR. WR6 is also the only regime that appears to have a prominent association with positive EMI conditions.

WR4 and WR6 are reduced in frequency when negative EMI conditions exist during winter through early summer (Figure 9a). When positive EMI conditions occur, there appears to be no appreciable response from WR4, but as previously mentioned there is a response for WR6 during mid-winter through early summer and again for summer through early autumn (Figure 9b). WR2 is greatly reduced in frequency during mid-summer through mid-autumn when negative EMI conditions exist.

3.6 Weather regime impacts on South Pacific rainfall

The correlation between WR frequency and GPCP rainfall anomalies (1979 – 2014; all months combined) shows spatially distinct patterns across the SW Pacific region and outside the Pacific basin (Figure 10a-f). WR1 and WR3 (Figure 10a and 10c, respectively) are previously ascribed as belonging to two distinct types of La Niña (Figure 5 and Figure 8); yet again, these two regimes exhibit subtly different tropical

and extra-tropical correlation patterns. For WR3 the SPCZ is inferred to move south and west of normal based on negative correlations (drying) in a diagonally-orientated zone aligned to the location where the SPCZ normally sits, coupled with positive correlations (relative wetting) near the Maritime Continent, the Coral Sea, and over New Caledonia. Conversely, the GPCP correlation maps (Figure 10f) indicate WR6 (shown as the opposite of WR3, see Figure 5 & 6) has the most prominent, large-scale positive rainfall anomalies spread across the SW Pacific tropics, but also suggests distinct dry anomalies occur in the area around the Coral Sea, New Caledonia and in the subtropical zone around the International Date Line (encompassing Fiji, Tonga and Niue). Positive rainfall correlations associated with WR6 indicate enhanced precipitation along the Equator around and east of the IDL and decreased rainfall over the Maritime Continent and in the southwest Pacific (from Papua New Guinea southeast to east of Fiji). The correlation field for WR6 suggests the SPCZ shifts north and east of normal. WR1 indicates relative drying occurs within regions usually occupied by both the ITCZ and SPCZ (Figure 10a). WR4 strongest correlations suggest it is associated with an enhanced ITCZ (Figure 10d), which is not surprising given the associated geopotential height anomalies that comprise this regime (Figure 6). WR4 frequency increases are associated with increased rainfall parallel to the northern side of the Equator from the Maritime Continent to about 110˚W and decreased precipitation south of the Equator from about the International Date Line east to South America (Figure 10d). WR2 has a strong positive and negative precipitation ‘dipole’ correlation signature that is localized between the Coral Sea and French Polynesia (Figure 10b). WR2 is also associated with

the strongest rainfall anomalies along the Equator for areas east of the International Date Line, along with WR6. The correlations for GPCP rainfall anomalies associated with WR5 are mostly near normal over most of the SW Pacific tropics, and any appreciable correlation anomalies are confined to the subtropical and mid-latitudes of the south Pacific basin (Figure 10e).

Local *in situ* rainfall variability at a seasonal level can be connected to weather regime frequency changes (Figure 11). Using a network of stations with high-quality rain data for austral summer (December, January, February) spanning the SW Pacific domain (and some sites just outside of it; Cairns, Townsville, Sydney and Kaitaia), distinct spatial patterns are observed for seasonal rainfall correlations to each regime (Figure 11). The strongest correlation of rainfall at any one site to a regime was observed for Hiva ‘Oa in the Marquesas and WR6 (Figure 11f), closely followed by Salote (Tonga) and WR3 (Figure 11c). Of the selected island rainfall analyzed in this study, Takaroa (in the Tuamotu Archipelago) shows a significant correlation to four WRs during summer, and most other island rainfall-WR correlations are significant for one to three WRs (with the surprising exception of Tahiti). Based on the number of sites that had significant correlations between WR occurrence and *in situ* rainfall totals, WR3 and WR6 appear to be the most important across the region, followed by WR2 and WR1. WR5 only appears to have an important effect for summer on Apia rainfall, and WR4 has no significant correlation to any of the stations assessed in this study. The poorest correlations between *in situ* rainfall totals and WR frequency for the analyzed sites were

observed for Cairns, Townsville, Sydney and Kaitaia. Overall, the variable strength of these correlations indicate that any one regime may or may not play a strong role in the overall variability of summer season rainfall at any given site we analyzed (in some cases, it is strong, while others it is weak).

However, when *in situ* island rainfall anomalies were aggregated by decile of WR occurrence (D1 indicates the lowest regime frequency and vice versa for D10), the average percent of normal seasonal rainfall illustrates stark outcomes for dryness and wetness in response to weather regime changes (Figure 11). We do not isolate the impact of any one WR on the rainfall anomalies here, and recognize that they co-occur to bring about seasonal climate conditions. However, what emerges from this analysis is that WR occurrence plays a strong role in dictating extreme seasonal rainfall for some SW Pacific locations. The greatest differences between average summer rainfall anomalies associated for D1 and D10 WR occurrence is observed for Hiva ‘Oa (Marquesas) in response to changes in WR1, 4, 5 and 6, , for Noumea (New Caledonia) in response to WR3, and for Tarawa (Kiribati) in response to WR 2 changes. The strongest negative rainfall anomalies in response to a overall regime increase occurs for Tarawa (with an average of 25% normal DJF rainfall) when WR3 is greatly increased, while the strongest positive rainfall anomalies are observed for Hiva ‘Oa (with an average of 228% normal DJF rainfall) in association with increased occurrence of WR6.

4. Discussion

4.1 Association of weather regimes with ENSO

The repeated affinity propagation exercise has reduced daily weather in the SW Pacific domain to six recurrent WRs (Figure 1) that have been analyzed in this study. We demonstrate that some of the regimes (Figure 2), but not all, appear sensitive to oceanic and atmospheric components of ENSO activity. We also observe that there is a phase-locking of some WR to the annual cycle (Figure 3). However, some of the characteristic traits seen in climate field correlations that are related to each of the regimes (Figure 5 & 6) appear unrelated to ENSO, and may therefore suggest that they arise from other climate modes (see following section) or internal atmospheric variability.

The spatial expression for WR1, 3, and 6 weather regimes to SST in patterns that are akin to those seen for ENSO (e.g. Allan et al., 1996) strongly suggests that (unsurprisingly) ENSO is a major contributor to WR variability in the SW Pacific. The connection of some WRs to ENSO reflects the SW Pacific geographic domain choice that was made in this study (see Supplemental Figures), and the overlap of the domain with core regions of ENSO operation - namely the NIÑO3.4 zone, the eastern edge of the Indo-Pacific Warm Pool and one of the atmospheric poles of the Southern Oscillation. Our reasoning for this domain choice was to locate the SPCZ in the middle of the field of analysis because of its relevance to small Pacific Islands. It is also evident that some WR occurrences and their climatological characteristics (Figure 3) are related

to the growth and decay of ENSO events (McPhaden et al., 2006). For instance, the regimes that are associated with CEI ENSO (WR3, WR6 and to a lesser extent WR1; see Figure 8) exhibit a rise and fall of frequency as well as self-persistence (Figure 4c) that are locked to the annual cycle, which is also known to modulate the strength of ENSO with a similar timing.

Two "opposite" weather regimes appear closely linked to CEI ENSO (WR3; "*TNT*" and WR6; *"TFP";* Figure 2). They show highly, but not exactly, contrasting spatial correlation patterns (Figures 5, 6 and 10). The contrasts between the CEI-based and EMI-based analyses (Figures 8 & 9) also suggest ENSO forcing of WR frequency changes are probably more prevalent when linked ocean-atmosphere situations are strongest during spring through autumn (i.e. when both atmospheric and oceanic anomalies related to ENSO are prevalent). For Equatorial Pacific ocean-dominated ENSO events (as with La Niña Modoki), autumn through early summer WR changes may be more common (Figure 8). In the latter situation, however, we note that there is not an "opposite" regime that has been identified as a counterpart to what associate with La Niña Modoki (WR1; *"HSP"*); however this could be due to the choice of restricting our analysis domain to the central-western Pacific (i.e. if the far eastern Pacific had been included, then perhaps El Niño Modoki may have emerged).

There is a discernable ENSO connection for WR1 during austral winter when SOI NIÑO and SOI NIÑA conditions exist. Despite WR1 also having strong SST

correlations nearly equivalent to WR3 across the Equatorial Pacific (Figure 7), the main differentiation between those two regimes relates to regional atmospheric features (Figure 2), which is also reflected in wider geopotential height correlation patterns (Figure 6). The differences between the spatial correlation fields for these two weather regimes are strikingly similar (and correspond to other metrics) ascribed recently by Song et al. (2016) for two types of La Niña; and as such we relate WR1 as arising more frequently during central-Pacific La Niña and WR3 increases as related to eastern Pacific La Niña events.

Distinct spatial differences for the WR impacts on *in situ* rainfall (Figure 11) are likely connected to associated movements of the ITCZ and SPCZ, which are respond to the SW Pacific atmospheric circulation (see Lorrey et al., 2012a for summer rainfall patterns linked to CEI phases). In addition, subtle differences between ENSO flavors are known to modulate region-wide tropical cyclone characteristics (Diamond et al., 2013). Therefore, ENSO should realistically play a significant role in the wider spatial patterns that are associated with the weather regimes, while also helping to dictate the specific rainfall anomalies for different small island nations in the SW Pacific region (Figure 10). Further work to examine inter-annual variability on the WR impacts and specific orographic signatures is also warranted.

4.2 Extra-basin and extra-tropical influences on SW Pacific atmospheric weather regimes

In some cases, the correlation maps for z850 and SSTa show subtle spatial pattern characteristics that appear similar to the signatures of known climate phenomena, and strong signatures outside of the tropical Pacific region. This indicates that climate driver influences from outside the Pacific basin may contribute to SW Pacific WR formation, and these drivers may result in influences on regional weather via teleconnections (Liu and Alexander 2007), but further work would be required to establish the physical mechanisms that potentially support them. A brief elaboration based on the observed spatial fields (Figure 5 and Figure 6) for WR2 and WR5 is provided in this discussion in light of prior work that demonstrates multiple climate driver teleconnections from distal sources can affect some Pacific weather types (Jiang et al., 2013).

In the z850 correlation field that is associated with WR2 (Figure 6b), an increase in regime frequency is concurrent with higher-than-normal geopotential heights over the entire Indian Ocean Basin, the Maritime continent and the Indo-Pacific Warm Pool (as well as New Zealand) with strong low pressure northeast of New Zealand. This geopotential height pattern appears similar to what develops at the tail end of the Madden-Julian Oscillation, so we examined WR2 frequency changes and the MJO index. WR2 is significantly increased (frequency nearly doubled) during MJO Phase 7 (Figure 12), suggesting it is triggered as MJO convective pulses enter the Pacific Basin. The correspondence of the geopotential height signatures for WR2 (seen in Figure 2 and

Figure 6) and increases in associated rainfall in the tropics and subtropics (where outgoing longwave radiation signatures are negative for MJO Phase 7; Figure 12) lends to the assertion that WR2 arises largely from the end of discrete MJO cycles as they draw to a close in the SW Pacific (Wheeler and Hendon, 2004).

WR5 also has a strong 'high' centered in the Ross Sea sector, and climatologically this regime occurs with greater frequency during late austral autumn (May) through mid austral spring (October). The mid-to-high latitude expression of the z850 correlation field for the New Zealand and Ross sea sector of the Southern Ocean (Figure 6e) suggests this may represent a Southern Annular Mode influence on WR5, (Fogt and Bromwich, 2006; Fogt et al., 2011; 2012). Correlations for SST appear weak outside of the Pacific Basin, but those signatures that are strong suggest in-flow of warmer SST into the North Tasman Sea via the East Australian Current would inhibited, promoting cooler waters, when WR5 occurs because of the southerly wind stress that is applied across the Tasman Sea sector. There are also aspects of the WR1 spatial correlations that are reminiscent of SAM (with regard to a broadly annular pattern circumscribing Antarctica) that are reminiscent of what can occur in concert with La Niña.

WR3 and WR6 (connected to ENSO; see previous section) also both exhibit an significant Antarctic dipole z850 correlation pattern that is positioned in a configuration reminiscent of the Pacific South American mode (PSA; Mo and Paegle, 2001). The PSA typically exhibits a see-saw in atmospheric mass between the Amunsden-Bellinghausen

sector west of the Drake Passage and the South Indian Ocean-western Ross Sea sector of the Southern Ocean along the Antarctic continent margin. This association is not surprising, but future work that focuses on the relationships between SW Pacific weather regimes and climate drivers external to the Pacific basin would help shed more light on these possible linkages. In addition, further analysis of how low-, mid-, and high-latitude synoptic types transition between one another, and their lead and lag relationships may help better understand potential atmospheric teleconnections and predictability on sub-seasonal time scales.

5. Conclusions

The k-means clustering analysis applied to daily near-surface geopotential fields has allowed a basic categorization and characterization of SW Pacific atmospheric weather regimes (Figure 2). The WR are important as they are 'attractors' for discrete types of weather (dry, wet, warm, cool, etc.). When aggregated over monthly and longer time scales (Ghil and Roberstson, 2002), weather regimes appear capable of producing significant seasonal climate impacts for small Pacific islands (droughts, pluvials, etc.). We have illustrated that a significant proportion of the WRs are related to ENSO, to fundamental global atmospheric circulation properties (Hadley and Ferrell circulation), and to drivers outside of the Pacific Basin (MJO, PSA, SAM). There are not always diametrically opposite occurrences of WR changes for different flavors of ENSO, and there is not always a single climate phenomenon that is responsible for a weather

regime waxing and waning in importance over the course of the annual cycle. Complex interplays of several climate modes and climate teleconnections outside of the tropical Pacific clearly help to exert important influences on SW Pacific weather types. Nevertheless, the classification that has been established in this study will allow a link between these regimes and distinct rainfall outcomes for Pacific Islands in future studies, which is expected to assist weather and seasonal climate forecasting of extreme precipitation (Kruk et al., 2015), temperatures for sea surface and land, as well as wind flow patterns.

An additional application of this study is toward regional palaeoclimate reconstruction efforts that employ atmospheric circulation regimes for integrating disparate climate archive signals (Lorrey et al., 2007; 2008; 2012b; Goodwin et al., 2013; Lorrey et al. 2014a; Browning and Goodwin, 2015). As such, the WR classification produced here is expected to assist hemisphere-wide palaeodata interpretation where large data sets are employed (see Past Global Changes (PAGES) 2k effort of Ahmed et al., 2013 for a recent example as well as the International Quaternary Union (INQUA) supported Southern Hemisphere Assessment of PalaeoEnvironments (SHAPE) international focus group). Moreover, extensive evidence demonstrates significant terrestrial, marine and human changes occurred across the Pacific region during the last millennium that may be due to weather and climate variability (Browning et al., 2015), however connections of past changes in weather to climate processes have been underdeveloped. The continued effort to link archaeological records to local climate reconstructions that can

provide meaningful insight about knock-on impacts to subsistence economies has previously proved difficult as well, in part, because Pacific data are widely-spaced and are relatively limited across Oceania. The advances made from this work, when applied to emerging regional palaeoclimatology proxy data and archaeology data networks, may also help to highlight the changeable influences of ENSO, extra-tropical and extra-Pacific basin climate processes and dynamics on Pacific Islands. Given the significant rainfall anomalies observed for the Marquesas, Samoa, Tonga and Tahiti station data used in this study, which all come from islands with rich records of pre-historic occupation and change (Allen, 2006), we would suggest future palaeoclimatology-archaeology linkages could be enhanced using a SW Pacific atmospheric weather regime context.

The outlook for ENSO activity under warming global conditions and the fate of the Pacific Islands from future ENSO impacts is not totally certain (Wang and Cai, 2013; Cai et al., 2015). However, some leading hypotheses indicate the surface and atmospheric variability associated with ENSO will increase (Fowler et al., 2012; Cai et al., 2012). As such, an interrogation of climate model simulation data that examines how weather regimes shift under different greenhouse gas representative concentration pathways (Collins et al., 2013) could provide a new perspective of what the future may hold for the SW Pacific. A WR interrogation of climate model simulations might also offer an additional perspective to assist in making large-scale atmospheric circulation patterns more compatible with small island scale climate responses, especially where

orographic influences are strong. In addition, SPCZ movements under future scenarios are notoriously variable in future simulations (Brown et al., 2012). Therefore, our suggestion to analyze WRs in climate model simulations may also assist in improving climate model selection or help to improve weighting for ensemble-based projections of future effective precipitation changes.

6. Acknowledgements

This work is a contribution to the Royal Society of New Zealand Marsden Fund project "Detecting prehistoric human-climate dynamics in central Polynesia using high-precision marine archives". Co-funding for AML and NCF time for analysis also came from the NIWA core-funded project "Climate Present and Past" project CAOA1701 and NOAA support for "The South Pacific Rainfall Atlas (SPRAT)". John-Mark Woolley is thanked for processing rainfall data.

7. References

Ackerley, D., Lorrey, A., Renwick, J.A., Phipps, S.J., Wagner, S., Dean, S., Singarayer, J., Valdes, P., Abe-Ouchi, A., Ohgaito, R. and Jones, J.M., 2011. Using synoptic type analysis to understand New Zealand climate during the Mid-Holocene. *Climate of the Past*, *7*(4), pp.1189-1207.

Adler, R.F., Huffman, G.J., Chang, A., Ferraro, R., Xie, P.P., Janowiak, J., Rudolf, B., Schneider, U., Curtis, S., Bolvin, D. and Gruber, A., 2003. The version-2 global precipitation climatology project (GPCP) monthly precipitation analysis (1979-present). *Journal of hydrometeorology*, *4*(6), pp.1147-1167.

Allan, R., Lindesay, J. and Parker, D., 1996. *El Niño southern oscillation & climatic variability*. CSIRO publishing.

Ashok, K., Behera, S.K., Rao, S.A., Weng, H. and Yamagata, T., 2007. El Niño Modoki and its possible teleconnection. *Journal of Geophysical Research: Oceans*, *112*(C11).

Baldwin, M.P. and Dunkerton, T.J., 2001. Stratospheric harbingers of anomalous weather regimes. *Science*, *294*(5542), pp.581-584.

Brown, J. R., Moise, A. F. & Delange, F. P. Changes in the South Pacific Convergence Zone in IPCC AR4 future climate projections. Clim. Dynam. 39, 1–19 (2012).

Browning, S.A. and Goodwin, I.D., 2015. The Paleoclimate reanalysis project.*Climate of the Past Discussions*, *11*, pp.4159-4204.

Cai, W., Lengaigne, M., Borlace, S., Collins, M., Cowan, T., McPhaden, M.J., Timmermann, A., Power, S., Brown, J., Menkes, C. and Ngari, A., 2012. More extreme swings of the South Pacific convergence zone due to greenhouse warming. *Nature*, *488*(7411), pp.365-369.

Cai, W., Santoso, A., Wang, G., Yeh, S.W., An, S.I., Cobb, K.M., Collins, M., Guilyardi, E., Jin, F.F., Kug, J.S. and Lengaigne, M., 2015. ENSO and greenhouse warming. *Nature Climate Change*.

Capotondi, A., Wittenberg, A.T., Newman, M., Di Lorenzo, E., Yu, J.Y., Braconnot, P., Cole, J., Dewitte, B., Giese, B., Guilyardi, E. and Jin, F.F., 2015. Understanding ENSO diversity. *Bulletin of the American Meteorological Society*, *96*(6), pp.921-938.

Cassou, C., 2008. Intraseasonal interaction between the Madden–Julian oscillation and the North Atlantic oscillation. *Nature*, *455*(7212), pp.523-527.

Collins, M., R. Knutti, J. Arblaster, J.-L. Dufresne, T. Fichefet, P. Friedlingstein, X. Gao, W.J. Gutowski, T. Johns, G. Krinner, M. Shongwe, C. Tebaldi, A.J. Weaver and M. Wehner, 2013. Long-term Climate Change: Projections, Commitments and Irreversibility. In: Climate Change 2013: The Physical Science Basis. Contribution of Working Group I to the Fifth Assessment Report of the Intergovernmental Panel on Climate Change [Stocker, T.F., D. Qin, G.-K. Plattner, M. Tignor, S.K. Allen, J.

Boschung, A. Nauels, Y. Xia, V. Bex and P.M. Midgley (eds.)]. Cambridge University Press, Cambridge, United Kingdom and New York, NY, USA

Diamond, H.J., Lorrey, A.M. and Renwick, J.A., 2013. A southwest Pacific tropical cyclone climatology and linkages to the El Niño–Southern Oscillation. *Journal of Climate*, *26*(1), pp.3-25.

Fauchereau, N., Pohl, B. and Lorrey, A., 2016. Extratropical Impacts of the Madden–Julian Oscillation over New Zealand from a Weather Regime Perspective. *Journal of Climate*, *29*(6), pp.2161-2175.

Fogt, R.L. and Bromwich, D.H., 2006. Decadal variability of the ENSO teleconnection to the high-latitude South Pacific governed by coupling with the Southern Annular Mode*. *Journal of Climate*, *19*(6), pp.979-997.

Fogt, R.L., Bromwich, D.H. and Hines, K.M., 2011. Understanding the SAM influence on the South Pacific ENSO teleconnection. *Climate Dynamics*,*36*(7-8), pp.1555-1576.

Frey, B.J. and Dueck, D., 2007. Clustering by passing messages between data points. *science*, *315*(5814), pp.972-976.

Gergis, J.L. and Fowler, A.M., 2005. Classification of synchronous oceanic and atmospheric El Niño-Southern Oscillation (ENSO) events for palaeoclimate reconstruction. *International Journal of Climatology*, *25*(12), pp.1541-1565.

Goodwin, I.D., Browning, S., Lorrey, A.M., Mayewski, P.A., Phipps, S.J., Bertler, N.A., Edwards, R.P., Cohen, T.J., van Ommen, T., Curran, M. and Barr, C., 2014. A reconstruction of extratropical Indo-Pacific sea-level pressure patterns during the Medieval Climate Anomaly. *Climate dynamics*,*43*(5-6), pp.1197-1219.

Hartigan, J.A., 1975. *Clustering algorithms*.

Jiang, N., Griffiths, G. and Lorrey, A., 2013. Influence of large-scale climate modes on daily synoptic weather types over New Zealand. *International Journal of Climatology*, *33*(2), pp.499-519.

Johnson, N.C., 2013. How many ENSO flavors can we distinguish?. *Journal of Climate*, *26*(13), pp.4816-4827.

Kalnay, E., Kanamitsu, M., Kistler, R., Collins, W., Deaven, D., Gandin, L., Iredell, M., Saha, S., White, G., Woollen, J. and Zhu, Y., 1996. The NCEP/NCAR 40-year reanalysis project. *Bulletin of the American meteorological Society*, *77*(3), pp.437-471.

Rousseeuw, P.J. and Kaufman, L., 1990. *Finding Groups in Data*. Wiley Online Library.

Kidson, J.W., 2000. An analysis of New Zealand synoptic types and their use in defining weather regimes. *International journal of climatology*, *20*(3), pp.299-316.

Kimoto, M., 1989: Multiple flow regimes in the Northern Hemisphere winter. Ph.D. thesis, University of California, Los Angeles, 210 pp. [Available from UCLA, Box 951575, Los Angeles, CA 90095-1575.].

Kruk, M.C., Lorrey, A.M., Griffiths, G.M., Lander, M., Gibney, E.J., Diamond, H.J. and Marra, J.J., 2015. On the state of the knowledge of rainfall extremes in the western and northern Pacific basin. *International Journal of Climatology*, *35*(3), pp.321-336.

Kug, J.S., Jin, F.F. and An, S.I., 2009. Two types of El Niño events: cold tongue El Niño and warm pool El Niño. *Journal of Climate*, *22*(6), pp.1499-1515.

Larkin, N.K. and Harrison, D.E., 2005. Global seasonal temperature and precipitation anomalies during El Niño autumn and winter. *Geophysical Research Letters*, *32*(16).

Lefèvre, J., Marchesiello, P., Jourdain, N.C., Menkes, C. and Leroy, A., 2010. Weather regimes and orographic circulation around New Caledonia. *Marine pollution bulletin*, *61*(7), pp.413-431.

Liu, Z. and Alexander, M., 2007. Atmospheric bridge, oceanic tunnel, and global climatic teleconnections. *Reviews of Geophysics*, *45*(2).

Lorrey, A. and Renwick, J. 2011. Assessment of the 2010-11 Southwest Pacific drought. NIWA client report AKL2011-036 prepared for the New Zealand Ministry of Foreign Affairs and Trade. 20 pp.

Lorrey, A., Fauchereau, N., Stanton, C., Chappell, P., Phipps, S., Mackintosh, A., Renwick, J., Goodwin, I. and Fowler, A., 2014a. The Little Ice Age climate of New Zealand reconstructed from Southern Alps cirque glaciers: a synoptic type approach. *Climate dynamics*, *42*(11-12), pp.3039-3060.

Lorrey, A. M., Griffiths, G., Fauchereau, N., Diamond, H. J., Chappell, P. R. and Renwick, J. 2014b. An ex-tropical cyclone climatology for Auckland, New Zealand. International Journal of Climatology, 34, 1157–1168.

Lorrey, A., Dalu, G., Renwick, J., Diamond, H. and Gaetani, M., 2012. Reconstructing the South Pacific Convergence Zone position during the presatellite era: A La Niña case study. *Monthly Weather Review*, *140*(11), pp.3653-3668.

Lorrey, A.M., Vandergoes, M., Almond, P., Renwick, J., Stephens, T., Bostock, H., Mackintosh, A., Newnham, R., Williams, P.W., Ackerley, D. and Neil, H., 2012. Palaeocirculation across New Zealand during the last glacial maximum at~ 21 ka. *Quaternary Science Reviews*, *36*, pp.189-213.

Lorrey, A., Fowler, A.M. and Salinger, J., 2007. Regional climate regime classification as a qualitative tool for interpreting multi-proxy palaeoclimate data spatial patterns: A New Zealand case study. *Palaeogeography, Palaeoclimatology, Palaeoecology*, *253*(3), pp.407-433.

Lorrey, A., Williams, P., Salinger, J., Martin, T., Palmer, J., Fowler, A., Zhao, J.X. and Neil, H., 2008. Speleothem stable isotope records interpreted within a multi-proxy framework and implications for New Zealand palaeoclimate reconstruction. *Quaternary International*, *187*(1), pp.52-75.

Matthews, A.J. 2012. A multiscale framework for the origin and variability of the South Pacific Convergence Zone. *Quarterly Journal of the Royal Meteorological Society*, 138, (666) 1165-1178.

McPhaden, M.J., Zebiak, S.E. and Glantz, M.H., 2006. ENSO as an integrating concept in earth science. *science*, *314*(5806), pp.1740-1745.

Michelangeli, P.A., Vautard, R. and Legras, B., 1995. Weather regimes: Recurrence and quasi stationarity. *Journal of the atmospheric sciences*,*52*(8), pp.1237-1256.

Mo, K. and Ghil, M., 1988. Cluster analysis of multiple planetary flow regimes. *Journal of Geophysical Research*, *93*(9), pp.10927-10952.

Mo, K.C. and Paegle, J.N., 2001. The Pacific–South American modes and their downstream effects. *International Journal of Climatology*, *21*(10), pp.1211-1229.

Moron, V. and Plaut, G., 2003. The impact of El Niño–southern oscillation upon weather regimes over Europe and the North Atlantic during boreal winter. *International Journal of Climatology*, *23*(4), pp.363-379.

Moron, V., Gouirand, I. and Taylor, M., 2015. Weather types across the Caribbean basin and their relationship with rainfall and sea surface temperature. *Climate Dynamics*, pp.1-21.

Moron, V., Gouirand, I., and Taylor, M. 2016. Weather types across the Carribean basin and their relationship with rainfall and sea surface temperature. *Climate Dynamics*, 47, 1-2, 601-621. DOI: 10.1007/s00382-015-2858-9

Park, H.S. and Jun, C.H., 2009. A simple and fast algorithm for K-medoids clustering. *Expert Systems with Applications*, *36*(2), pp.3336-3341.

Qian, W., Shan, X., Chen, D., Zhu, C. and Zhu, Y., 2012. Droughts near the northern fringe of the East Asian summer monsoon in China during 1470–2003. *Climatic change*, *110*(1-2), pp.373-383.

Renwick, J.A., 2011. Kidson's synoptic weather types and surface climate variability over New Zealand. *Weather and Climate*, *31*, pp.3-23.

Riddle, E.E., Stoner, M.B., Johnson, N.C., L'Heureux, M.L., Collins, D.C. and Feldstein, S.B., 2013. The impact of the MJO on clusters of wintertime circulation anomalies over the North American region. *Climate dynamics*,*40*(7-8), pp.1749-1766.

Saji, N.H. and Yamagata, T., 2003. Structure of SST and surface wind variability during Indian Ocean Dipole mode events: COADS observations*.*Journal of Climate*, *16*(16), pp.2735-2751.

Saji, N.H., Goswami, B.N., Vinayachandran, P.N. and Yamagata, T., 1999. A dipole mode in the tropical Indian Ocean. *Nature*, *401*(6751), pp.360-363.

Song, L., Chen, S., Chen, W., Chen, X. 2016. Distinct impacts of two types of La Niña events on Australian summer rainfall. International Journal of Climatology, 37, 2532-2544; DOI: 10.1002/joc.4863

Taschetto, A., Wainer, I. and Raphael, M., 2007. Interannual variability associated with Semiannual Oscillation in southern high latitudes. *Journal of Geophysical Research: Atmospheres*, *112*(D2).

Takahashi, K. & Battisti, D. Processes controlling the mean tropical Pacific precipitation pattern. Part II: The SPCZ and the Southeast Pacific Dry Zone. J. Clim. 20, 5696–5706 (2007).

Tziperman, E., Stone, L., Cane, M.A. and Jarosh, H., 1994. El Niño chaos: Overlapping of resonances between the seasonal cycle and the Pacific ocean-atmosphere oscillator. *Science-AAAS-Weekly Paper Edition-including Guide to Scientific Information*, *264*(5155), pp.72-73.

Vautard, R. and Legras, B., 1988. On the source of midlatitude low-frequency variability. Part II: Nonlinear equilibration of weather regimes. *Journal of the atmospheric sciences*, *45*(20), pp.2845-2867.

Vautard, R., 1990. Multiple weather regimes over the North Atlantic: Analysis of precursors and successors. *Monthly weather review*, *118*(10), pp.2056-2081.

Vincent, E. M. et al. Interannual variability of the South Pacific Convergence Zone and implications for tropical cyclone genesis. Clim. Dynam. 36, 1881–1896 (2011).

Wang, Guojian, and Wenju Cai. "Climate-change impact on the 20th-century relationship between the Southern Annular Mode and global mean temperature." *Scientific reports* 3 (2013).

Wheeler, M. and H. Hendon, 2004: An All-Season Real-Time Multivariate MJO Index: Development of an Index for Monitoring and Prediction. Mon. Wea. Rev., 132, 1917-1932.

Widlansky, M. J., Webster, P. J. & Hoyos, C. D. 2011. On the location and orientation of the South Pacific Convergence Zone. Clim. Dynam. 36, 561–578.

Wilks, Daniel S. 2011. *Statistical methods in the atmospheric sciences*. Vol. 100. Academic press.

Yeh, S.W., Kug, J.S., Dewitte, B., Kwon, M.H., Kirtman, B.P. and Jin, F.F., 2009. El Niño in a changing climate. *Nature*, *461*(7263), pp.511-514.

Yiou, P. and Nogaj, M., 2004. Extreme climatic events and weather regimes over the North Atlantic: When and where?. *Geophysical Research Letters*,*31*(7). 31, L07202, doi:10.1029/2003GL019119

Figure 1.

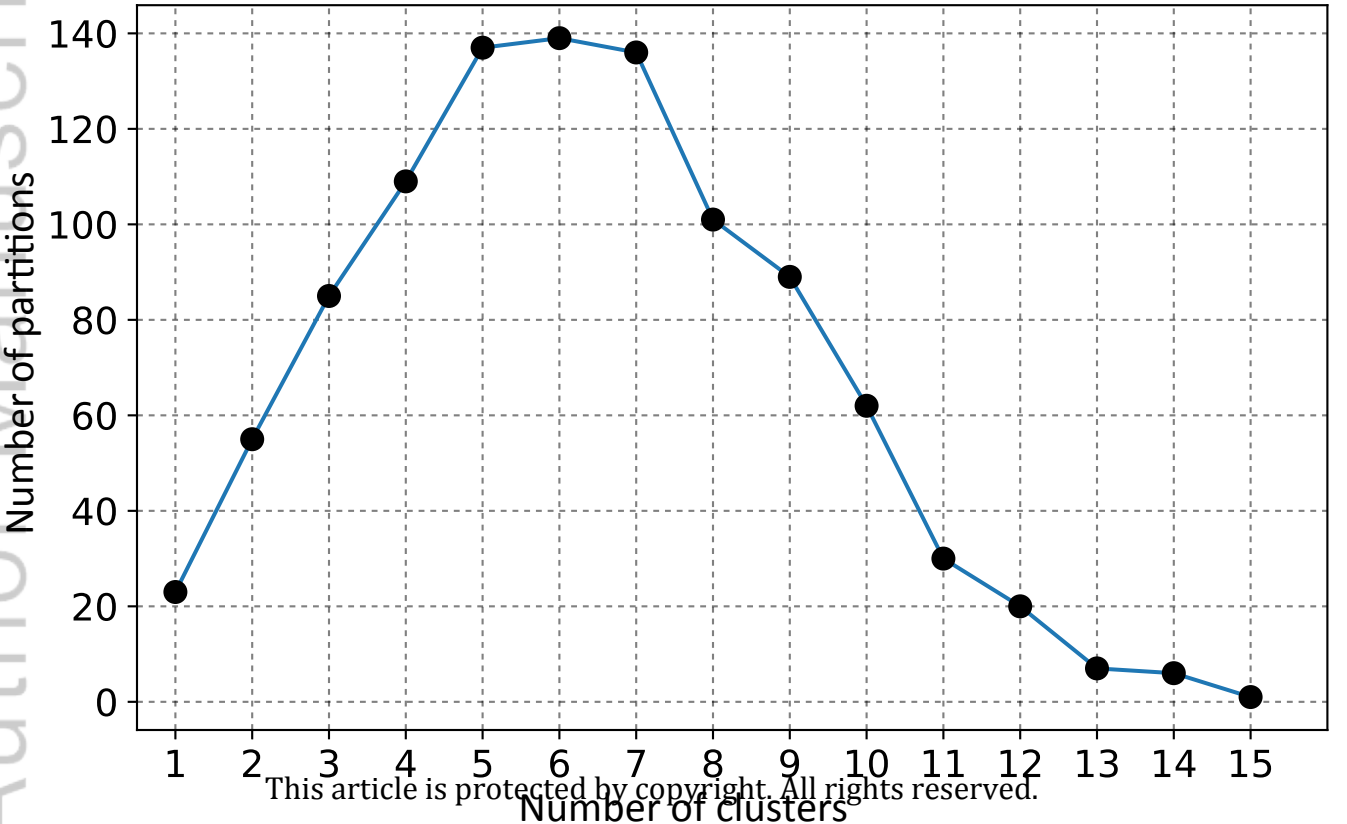

Figure 2.

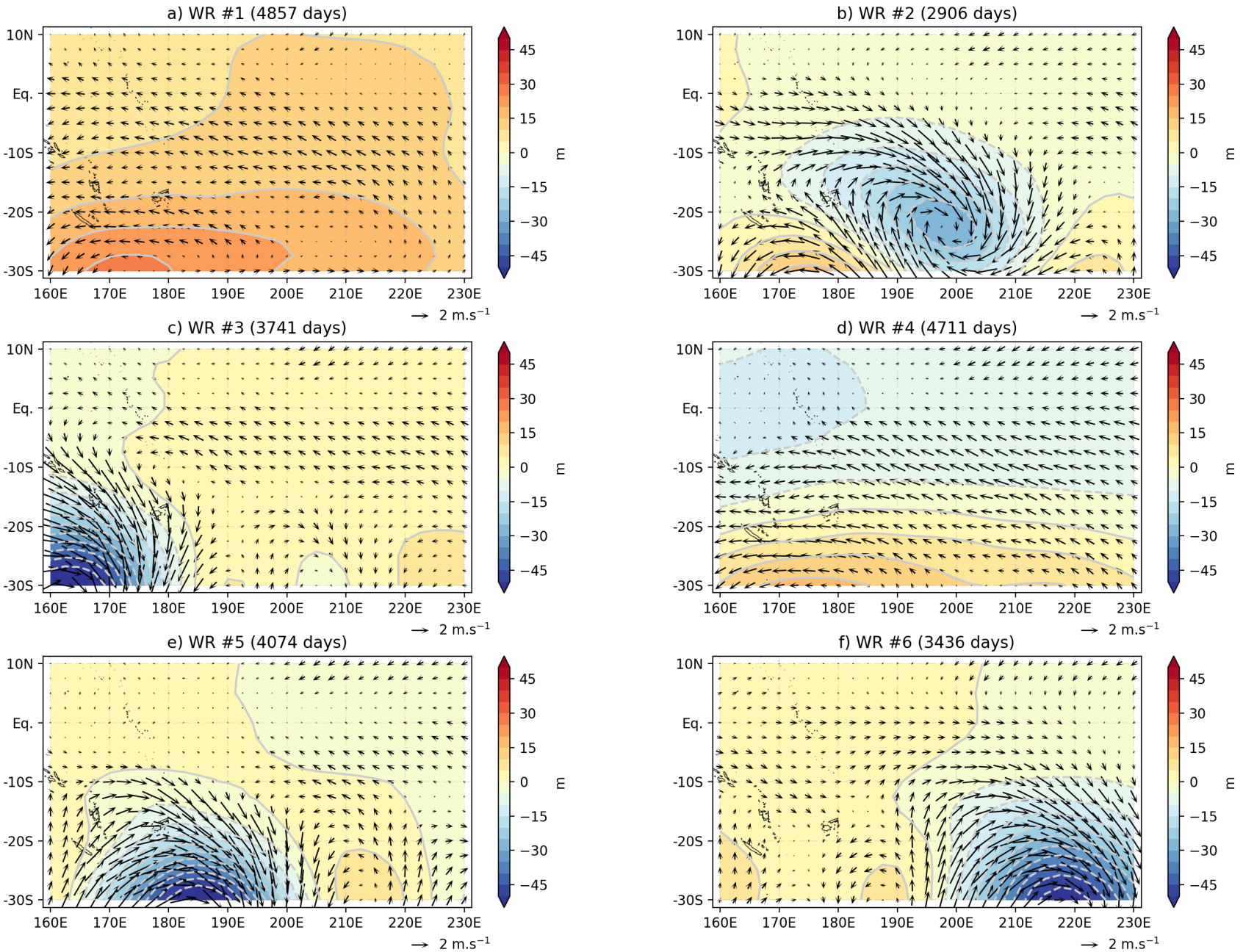

Figure 3

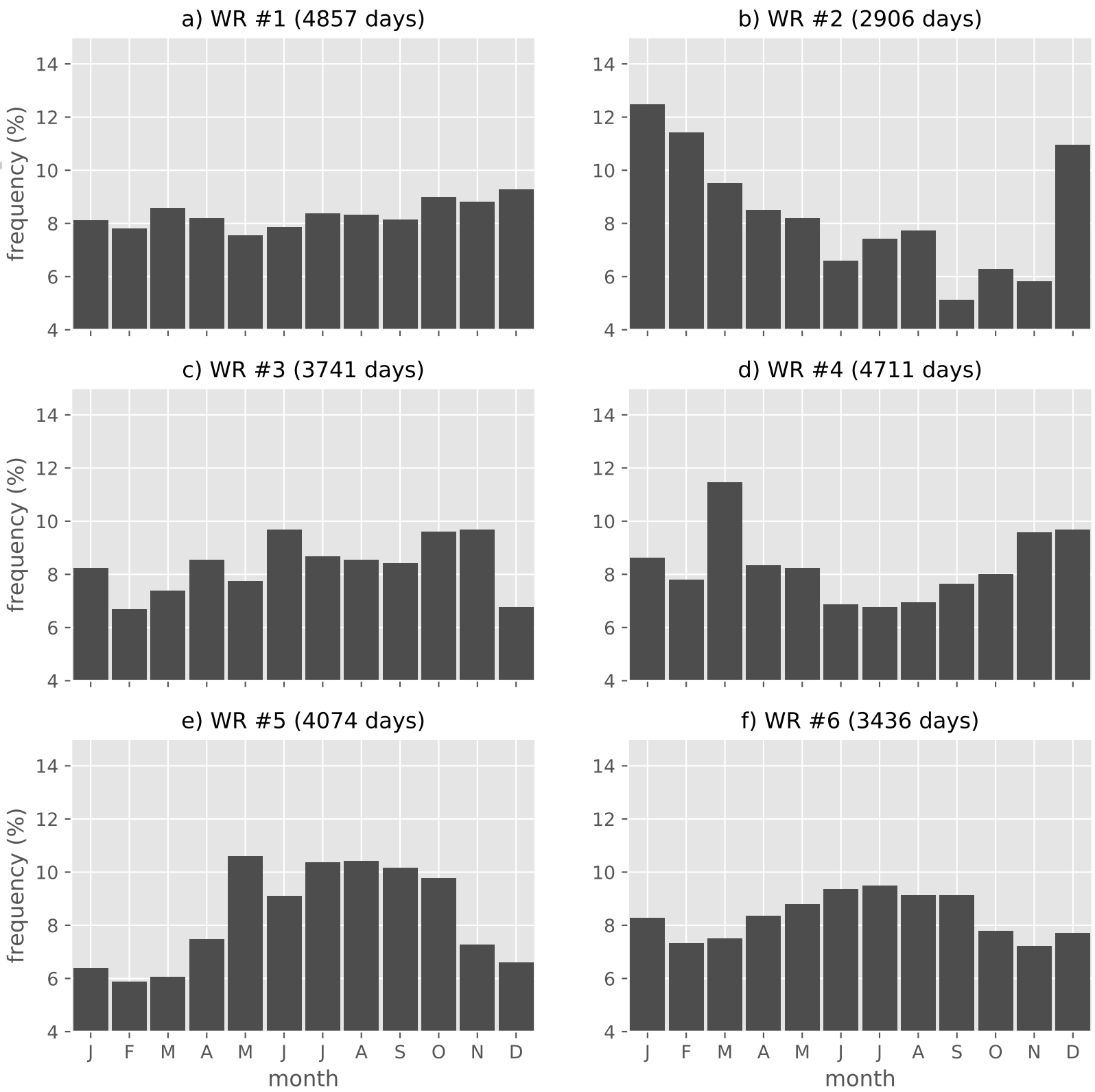

Figure 4

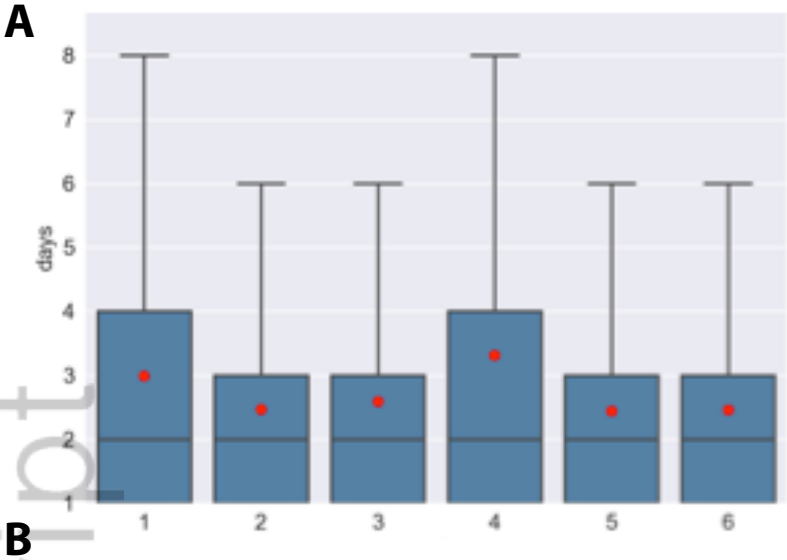

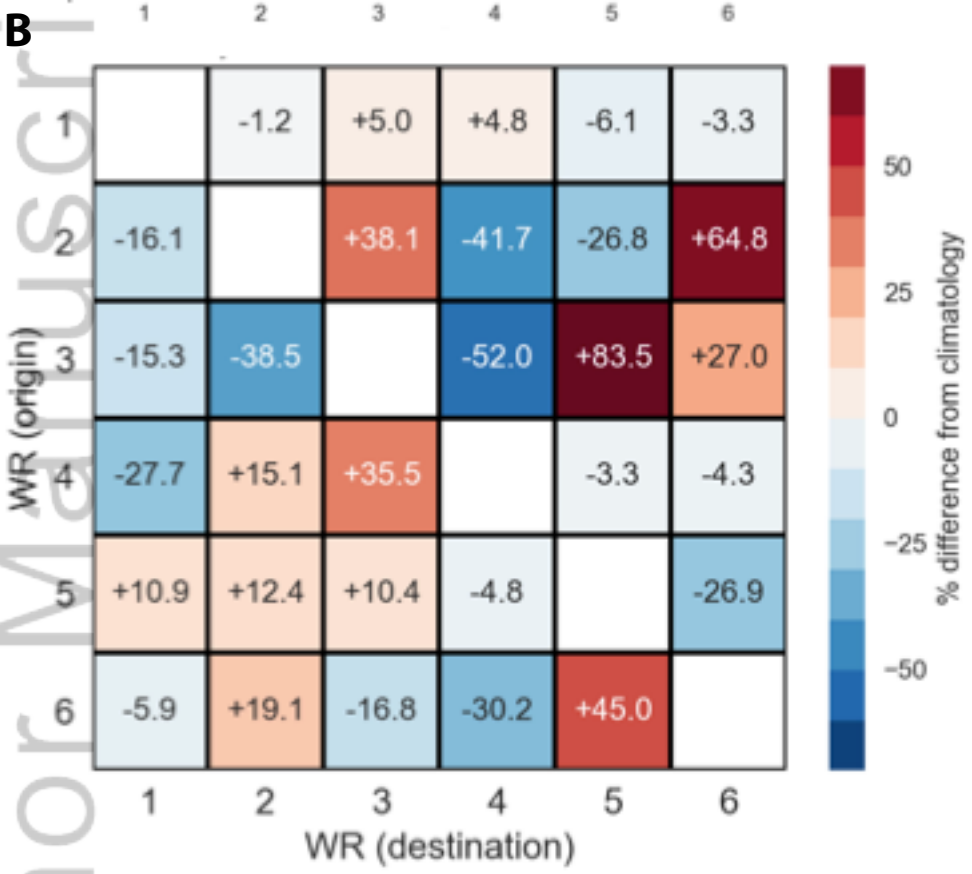

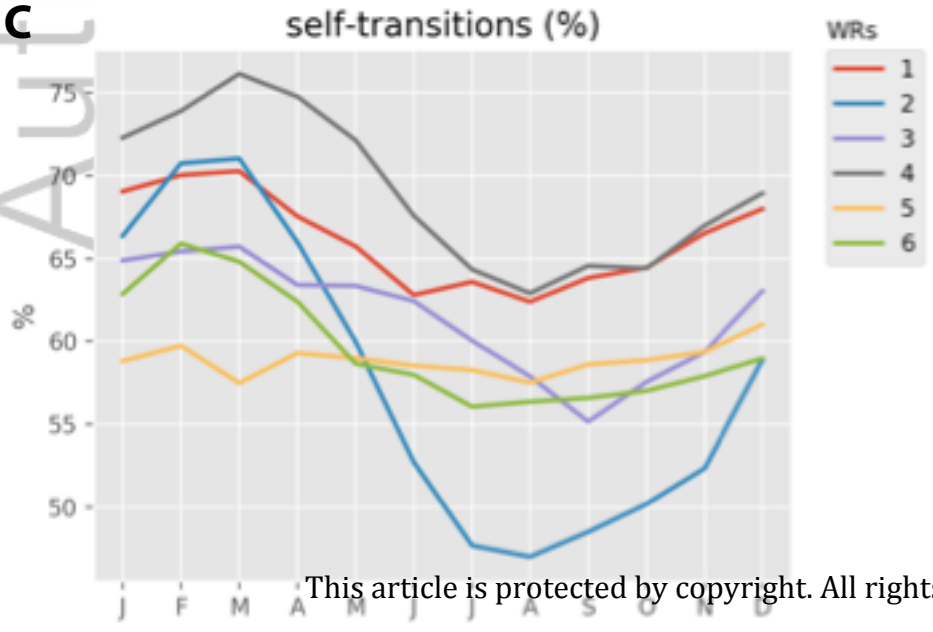

Figure 5

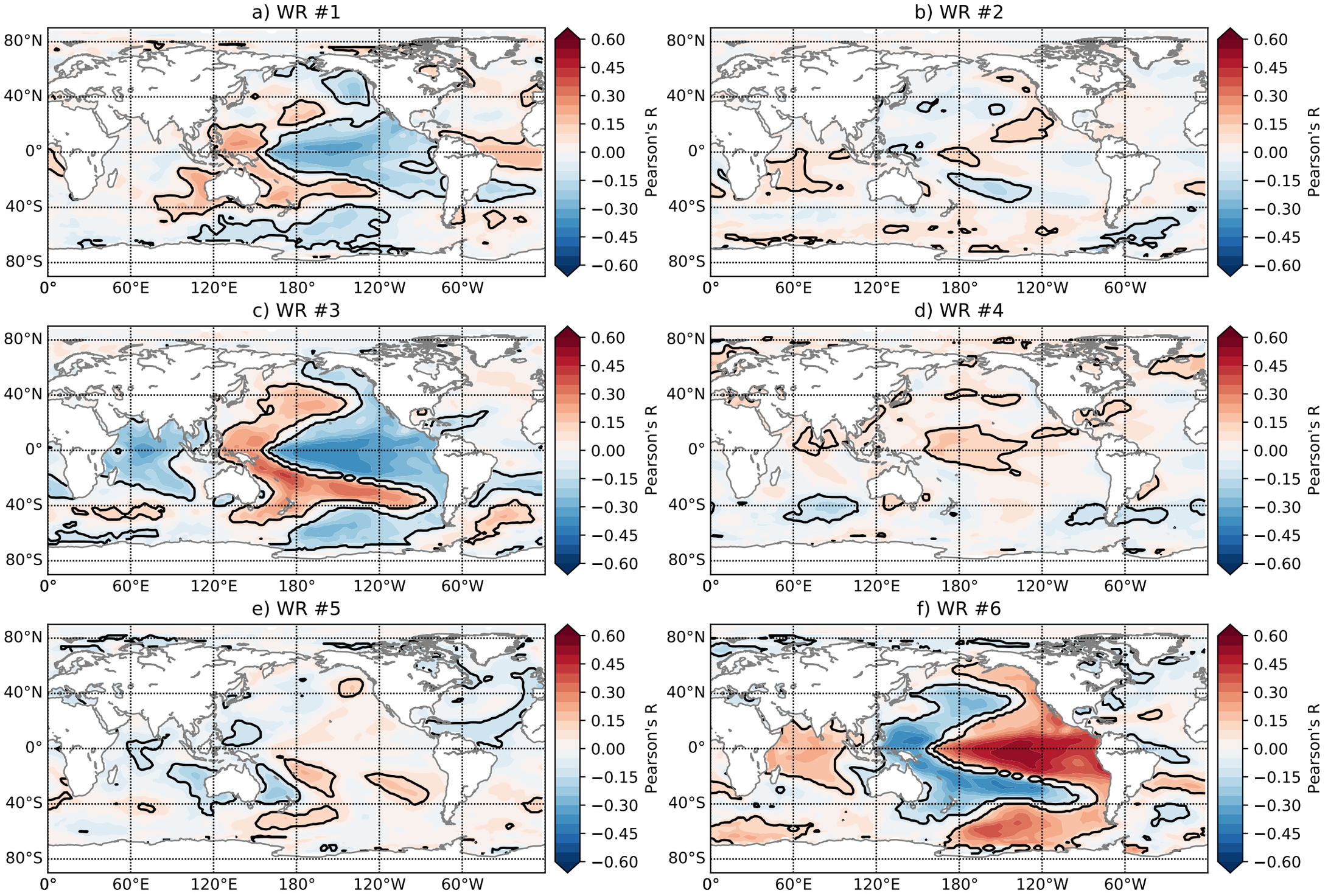

Figure 6

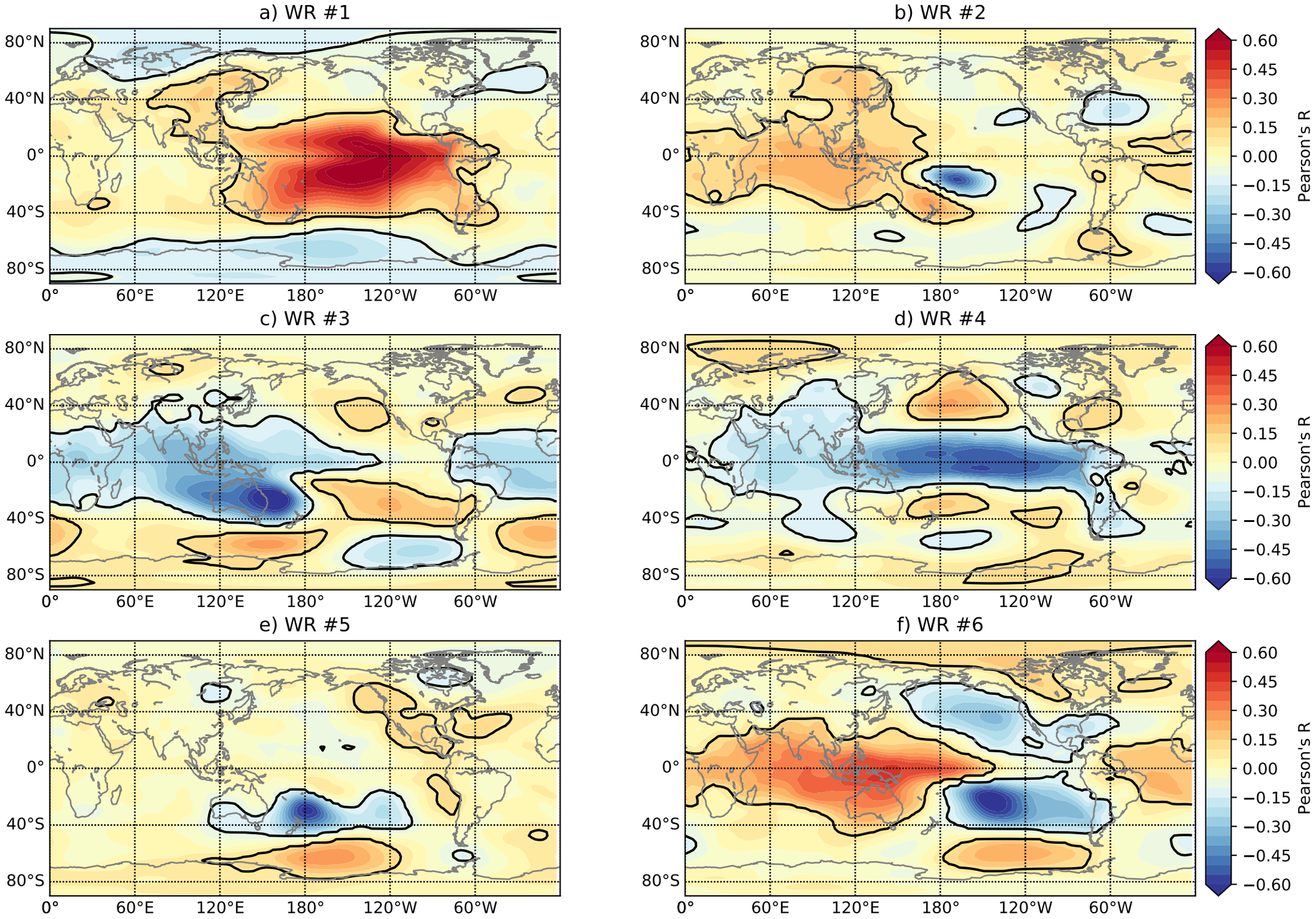

Figure 7.

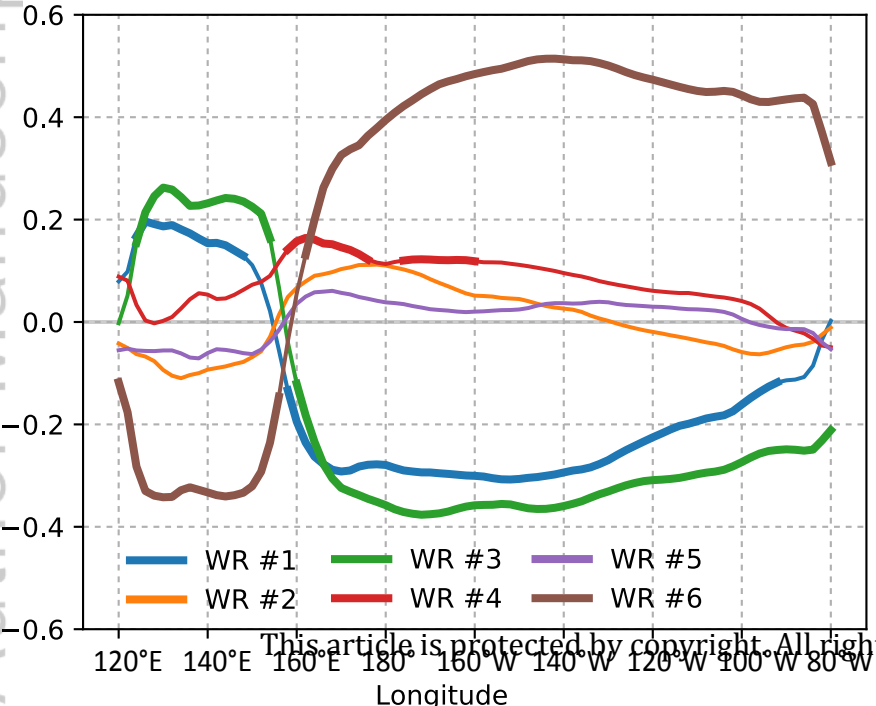

Figure 8

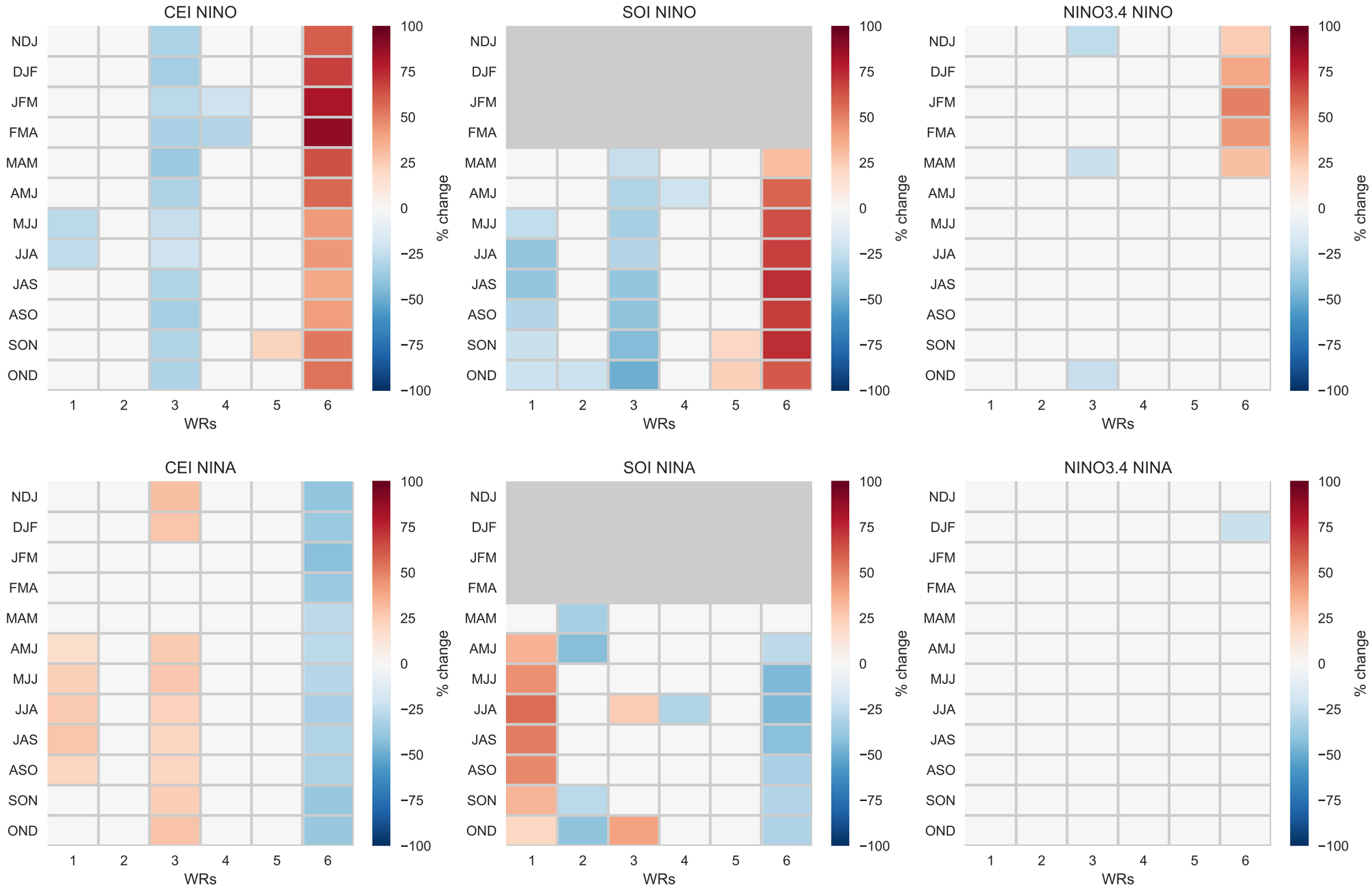

Figure 9.

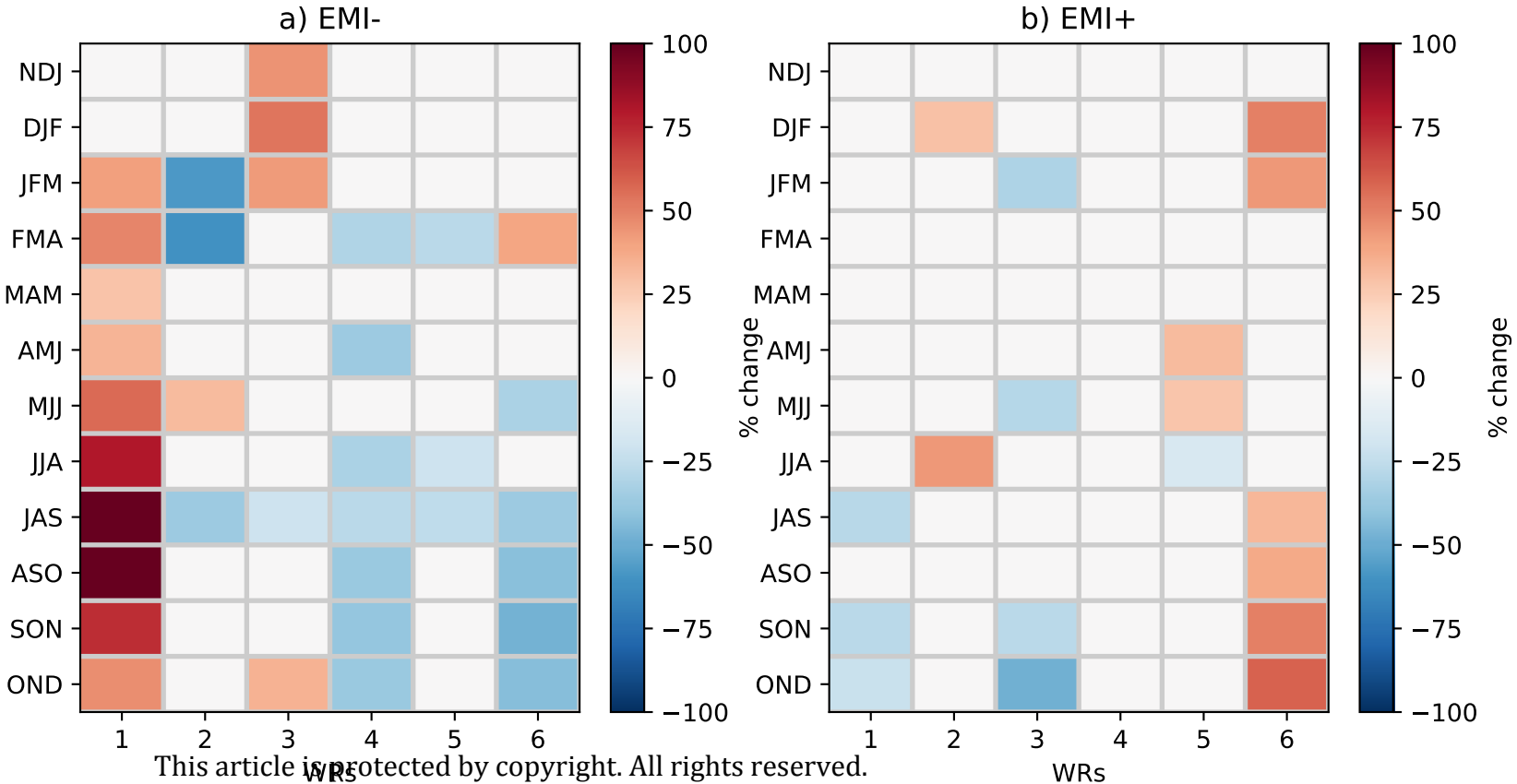

Figure 10.

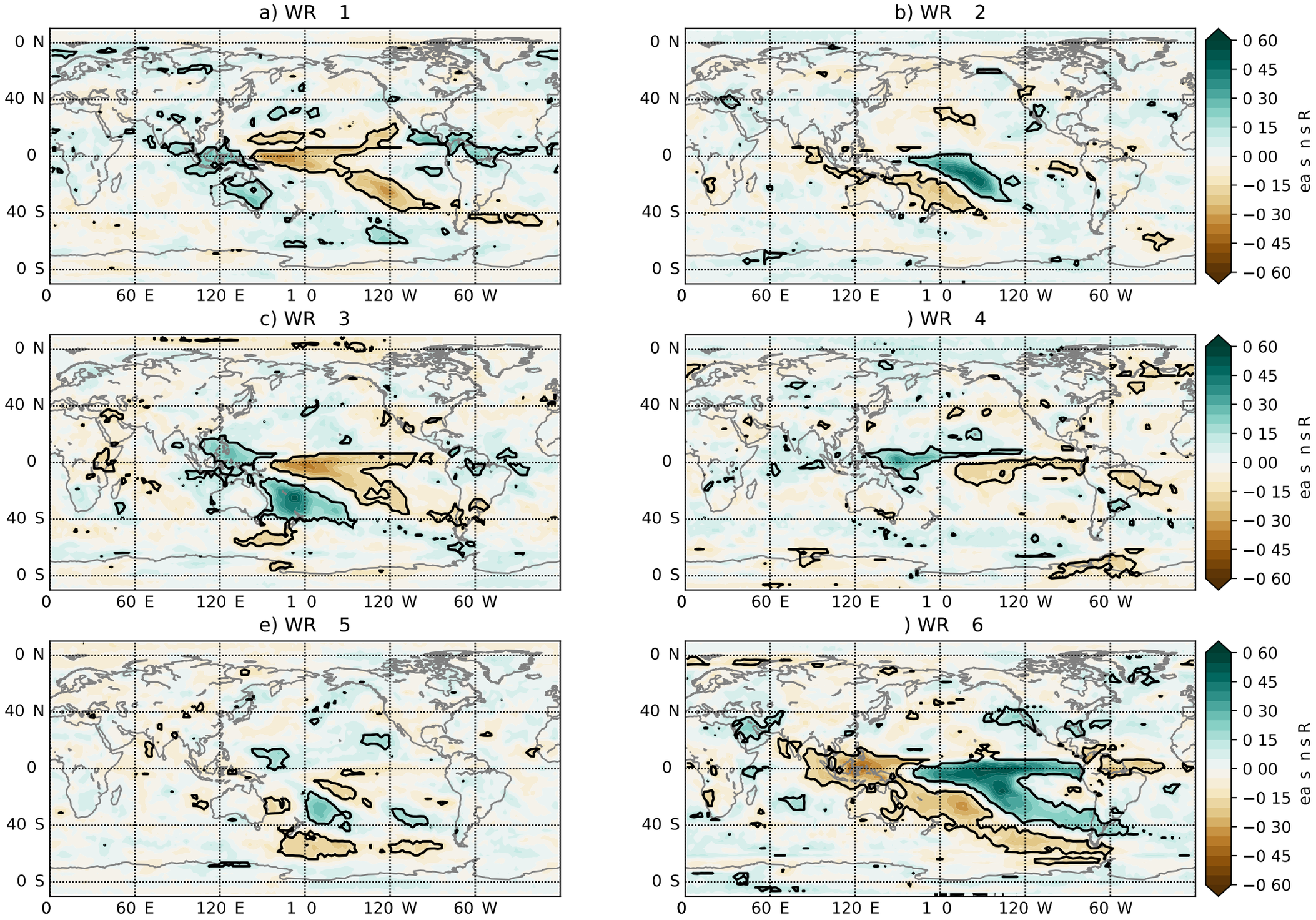

Figure 11.

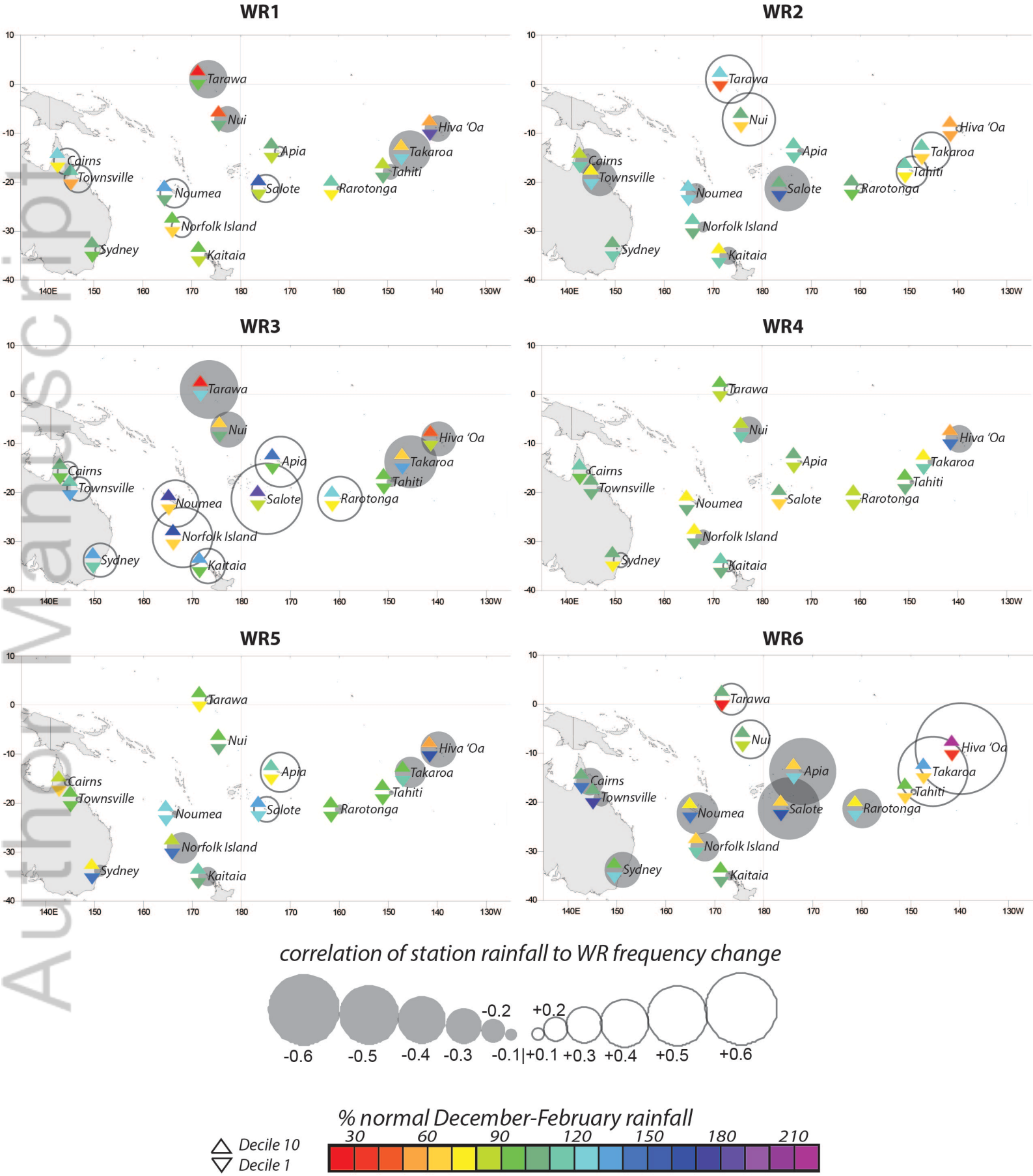

Figure 12.